

# An Efficient Three-Port Partial Power Converter Based EV On-Board Fast Charger

Radha Kushwaha<sup>ID</sup>, Senior Member, IEEE, Vinod Khadkikar<sup>ID</sup>, Fellow, IEEE, Shakti Singh<sup>ID</sup>, Member, IEEE, Hatem H. Zeineldin<sup>ID</sup>, Senior Member, IEEE, Rabeb Mizouni<sup>ID</sup>, and Hadi Otrok<sup>ID</sup>, Senior Member, IEEE

**Abstract**—The objective of this work is to design and develop a new three port boost AC-DC converter which facilitates on-board fast charging for electric vehicles using partial power processing (PPP) at bidirectional DC-DC stage. As compared to conventional two-stage chargers with two port AC-DC and full-power processing (FPP) DC-DC converter, the three-port converter (TPC) ensures reduced voltage stress across the switches. This allows the converter operation at higher power without additional stress on devices while reducing the charging time. The PPP at DC-DC stage makes it highly efficient due to reduced power conversion stages. The proposed TPC is able to generate three levels of output voltage, which reduces the converter switching loss. The proposed TPC with PPC concept further minimizes the power losses as only a fraction of the power is processed by the DC-DC converter switches and components. Hence, the charger overall size and cost can be reduced while achieving significantly high efficiency as compared to conventional two-stage charger with FPP, even without soft-switching. The performance of proposed charger is validated under different operating conditions using MATLAB/Simulink based simulation model for 6.6 kW and scaled down-lab prototype for 1.5 kW.

**Index Terms**—Electric vehicle, fast charging, partial power conversion, three-port converter, two-stage charger.

## I. INTRODUCTION

ELCTRIC vehicles (EVs), EV chargers are expected to be as fast as the fueling of the conventional fossil fuel-based vehicles [1]. To meet this expectation and since, the charging speed being the bottleneck for the wide adoption of EVs, the on-board and off-board chargers need to be designed efficiently, for higher charging current, i.e., higher power. However, for

Received 5 March 2024; revised 12 July 2024; accepted 12 August 2024. Date of publication 15 October 2024; date of current version 31 January 2025. Paper 2024-TSC-0210.R1, presented at the 2022 IEEE International Conference on Power Electronics, Drives and Energy Systems (PEDES), Jaipur, India, Dec. 14–17, and approved for publication in the IEEE TRANSACTIONS ON INDUSTRY APPLICATIONS by the Transportation Systems Committee of the IEEE Industry Applications Society [DOI: 10.1109/PEDES56012.2022.10080032]. This work was supported in part by the Khalifa University Competitive Internal Research Award under Grant CIRA-2019-070 (Award Number 8474000187) and in part by ASPIRE under the ASPIRE Virtual Research Institute Program, Award number VRI20-07. (Corresponding author: Radha Kushwaha.)

The authors are with the Department of Electrical Engineering and Computer Science, Khalifa University, Abu Dhabi 127788, UAE (e-mail: radha.kushwaha@gmail.com; vinod.khadkikar@ku.ac.ae; shakti.singh@ku.ac.ae; hatem.zeineldin@ku.ac.ae; rabeb.mizouni@ku.ac.ae; hadi.otrok@ku.ac.ae).

Color versions of one or more figures in this article are available at <https://doi.org/10.1109/TIA.2024.3481200>.

Digital Object Identifier 10.1109/TIA.2024.3481200

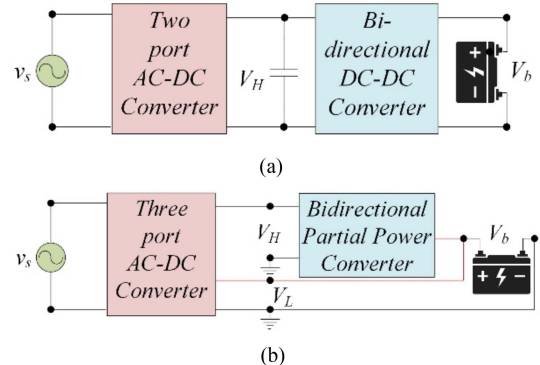


Fig. 1. General architecture of. (a) Conventional charger with FPP two-port converter, and (b) proposed fast charger with three-port converter.

on-board configuration, the high-power rating implies to increased size and cost of the AC-DC converter due to use of higher rating power devices [2]. Further, at high power, the losses are seen to be significant, which impacts the charger efficiency.

A comprehensive review on different AC-DC converter topologies applicable to conventional recent EV chargers, is given in [2]. The conventional on-board chargers are mostly designed for slow charging, due to limitation of voltage and current stress on devices. Fig. 1(a) shows the conventional two-stage charger configuration with two-port buck-boost converter followed by full power processing (FPP) DC-DC converter [3], [4]. The two-port converter maintains \$V\_H\$ at 300 V, which cascades the DC-DC stage for battery charging using constant current-constant voltage control. For 220 V single-phase AC system, the voltage stress in these two-port converters is typically in the range 400 V–500 V for AC-DC stage and in the range of 400–600 V (max) for DC-DC stage. This restricts the charger operation for high power resulting in low charging speed at the battery end. Moreover, for a given power, higher voltage rating switches are required for the implementation of two-port converter. Therefore, the cost and overall foot-print of the charger is generally high and efficiency still has margin to be improved further. The efficiency improvement in on-board chargers is achieved in three ways: by using single-stage/two-stage high gain configuration, by using soft-switching with full-power processing (FPP) DC-DC stage and by using the concept of partial-power processing at DC-DC stage. The efficiency improvement with single-stage/two-stage high gain

configuration [5], [6], [7] is not that significant, besides the input voltage range has to be restricted due to high gain configuration. Even with soft-switching, the peak efficiency for the recent EV chargers with FPP DC-DC conversion is seen to be in the range 93%–96% [8], [9], [10], [11]. Sharma et al. have presented many bidirectional two-stage chargers with FPP but with limited efficiency within the range 92–94% and with higher number of components [12], [13]. A single-stage bidirectional EV charger with FPP is reported in [14] with same number of device and components but the efficiency improvement of only 1% is seen. Moreover, the control for all these bidirectional chargers is complex and requires expensive controllers such as dSpace for the implementation. Further, the FPP DC-DC converter requires the higher current rating devices at the battery side, due to DC-DC converter designed at rated power, which again limits the overall charger efficiency, size and increases the cost. Therefore, to overcome the size, cost and efficiency limitations, a new fast charger configuration by using the concept of partial-power processing (PPP) at DC-DC stage, as shown in Fig. 1(b), is presented in this paper.

The recent literature on PPP converter present several DC-DC converter solutions applicable to EV fast chargers. However, most of these topologies employ HF transformer and large number of devices [15], [16]. As per SAE J1772 standard [17], considering the safety aspect, generally in electric vehicles, the battery ground is floating and separated from the power electronic ground, which is connected to the chassis of the vehicle. Therefore, the battery and the power electronic interface of the vehicle have different grounds. Therefore, the isolation transformer in conventional chargers can be eliminated and there is no need of isolated converter at DC-DC stage. The advantages of PPP concept at DC-DC stage in terms of size, cost and efficiency are discussed in detail in [18]. The concept of partial power processing for voltage step-up and step down, is popular in photovoltaic (PV) systems [19]. Further, several topologies based on series connected PPP converters have been reported in the literature [20] and also been applied for EV fast charging [21]. For fast charging, the concept of PPP is based on reducing the peak power (or current) handled by DC-DC stage, which is seen during constant current (CC) charging mode. Alternately, till the peak charging current requirement during CC mode is met by the converter, the converter output voltage can be a fraction of the battery voltage. Hence, the converter output voltage can be in series connection with the battery voltage, which is the main philosophy of PPP concept used in this work at DC-DC stage.

The literature on PPP achieves this connection in two different ways and hence, two PPP configurations namely, type-I and type-II are derived in the literature [20], [21]. Apparently, Type-I configurations are under step-down category and achieved with IPOS (Input-Parallel Output-Series) connection of battery, DC-link voltage and DC-DC converter terminals. At the input side, DC-DC topology is connected in parallel with the DC-link voltage and at the output side, the fraction of the battery voltage is connected in series with the DC-DC converter input (or DC-link voltage). The other Type-II configuration is another step-down

approach, which is achieved with ISOP (Input-Series Output-Parallel) connection of the battery, DC-link voltage and DC-DC converter terminals [20], [21]. To derive ISOP, at the output side, DC-DC topology output is connected in parallel to the battery voltage. However, the input port of the DC-DC topology is connected to the fraction of the battery voltage in series, as shown in Fig. 1(b). To charge the battery continuously, there is a direct path (or bypass connection) available, through which the fraction of the battery voltage is connected to the DC-DC converter input. This direct connection makes it possible to charge the battery using single-stage conversion, bypassing the DC-DC stage for most of charging cycle. Therefore, only a portion of battery power need to be handled by the DC-DC converter i.e., the DC-DC converter rating is reduced significantly, leading to high efficiency and significant reduction in size and cost.

Apparently, the combination of three-port AC-DC converter with PPP concept at DC-DC stage can help in minimizing the size, cost and efficiency issues further, which is the focus of this work. Fig. 1(b) shows the general architecture of proposed charger with three-port boost AC-DC converter, followed by bidirectional buck-boost PPP DC-DC converter. The distinctive feature of proposed charger is that most of the power is fed to the battery by three-port converter (TPC) directly, bypassing the DC-DC stage [22]. The proposed TPC offers the advantage of reduced device voltage stresses (i.e.,  $V_L$  and  $V_H - V_L$ ) due to the partial voltage available across the lower and upper port, respectively. This reduced device voltage stress allows the converter operation at higher power using the same switches, facilitating the fast charging at battery end. Therefore, the charging speed is seen to be more as compared to conventional two-port converter-based charger. Moreover, the lower voltage rating switches can be used at TPC stage to reduce the size of converter. Further, the DC-DC stage processes only a fraction of the full charging power, which significantly reduces the conversion stages, as compared to the conventional two stage charger, thereby, improving the charger efficiency. Moreover, due to reduced power processing, the current stress on DC-DC converter switches is very low. This facilitates the use of lower current rating switches for the bidirectional converter. Therefore, overall size and cost of the charger is reduced with higher efficiency. A detailed comparative analysis of proposed charger with PPP over the contemporary solution in literature [5], [6], [7], [8], [9], [10], [11], [12], [13] is given in Table I. The main contribution and novelty of this new TPC based charger with PPP concept are given below.

- The proposed charger with PPP concept facilitates increased charging rate, as compared to the conventional charger with full power processing.
- The use of PPP concept enhances the charger overall efficiency, as only a fraction of total power is processed by the DC-DC converter.
- The device voltage stress at TPC stage and the current stress of DC-DC converter is significantly low.
- The proposed TPC provides three levels of output voltage, which results into further reduced switching losses and improved efficiency.

TABLE I  
COMPARISON WITH OTHER CONTEMPORARY SOLUTIONS IN THE LITERATURE

Parameters	[5]	[6]	[7]	[8]	[9]	[10]	[11]	[12]	[13]	proposed
<b>Topology</b>	BL Cuk	BL buck-boost + Iso. Cuk	Modified sepic +Luo	IL buck boost+ sync HB conv.	Boost-buck	Boost-buck+PSF B	PFC+PSF B	1 ph pfc+iso cuk	1ph pfc+ iso. IL sepic	TP boost+bidi r. BB
<b>Use of PPP</b>	no	no	no	no	no	no	no	no	no	yes
<b>Switches</b>	2	4	2	6	2	7	10	6	8	4
<b>diodes</b>	2	6	4	2	6	11	4	0	0	2
<b>inductors</b>	2	4	3	3	2	4	3	2	2	2
<b>capacitors</b>	3	6	4	2		4	3	2	4	2
<b>Front-end DBR</b>	No	No	No	Yes	Yes	yes	No	No	no	yes
<b>Power rating</b>	1kW	1kW	650W	1kW	1kW	1kW	1.3kW	1kW	1kW	1.5kW
<b>Sensors</b>	1	3	1	2	3	5	4	4	5	2
<b>devices in current flow path</b>	1s+2d	2S+5D	3s+4d	3s+1d	2s+2d	4s+5d	5s+2d	4s+0d	6s+0d	3s+2d
<b>Input current</b>	continuo us	discontinuo us	continuo us	discontinuo us	continuo us	continuo us	continuo us	continuo us	continuo us	continuo us
<b>Switch utilization</b>	Medium	low	low	Low	low	Medium	High	high	high	high
<b>DC-link voltage switching</b>	400V	300V	300V	400V	150-450V	150-400V	120-450V	400V	400V	400V
<b>THD</b>	<5%	1.04-8.19%	<5%	<5%	<5%	NM	<5%	<5%	<5%	<5%
<b>Applicable power range</b>	medium	medium	Medium	medium	Medium	low	High	medium	high	high
<b>Switch voltage stress</b>	Low	High	High	High	high	medium	low	low	low	low
<b>Compatibility</b>	MV charging	MV charging	MV charging	MV charging	MV charging	LV &MV	MV charging	MV charging	MV charging	MV charging
<b>Switch current stress</b>	high	medium	medium	medium	medium	high	high	high	high	low
<b>efficiency</b>	94.2%	91-94%	94.5-95.5%	96.06%	96%	Nm	95.8%	90.18	89.81	96.7

- Due to reduced size of switches, charger size and cost can be lower as compared to conventional chargers [3], [4], [11].

## II. CIRCUIT CONFIGURATION, STEADY-STATE ANALYSIS AND DESIGN

The proposed charger consists a three-port boost AC-DC converter at front-end, followed by bidirectional buck-boost DC\_DC converter with partial power processing (PPP). As shown in Fig. 2(a), the circuit comprises a three-port AC-DC converter using switches  $S_w$ ,  $S_{wL}$ , diodes  $D_1$ ,  $D_2$  and inductor  $L_i$  with the DC-link capacitors  $C_H$  and  $C_L$ . This TPC is further connected in series with the bidirectional DC-DC converter using switches  $S_{b1}$ ,  $S_{b2}$  and inductor,  $L_b$ . For single-phase 220 V system, the bus voltage  $V_H$  is regulated at 400 V, however, the charging port  $V_b$  is controlled to provide 270 V. Mostly, the lower port  $V_L$  directly transfers the charging power to the battery, using a bypass connection (red line). This directly transferred power largely depends upon the ratio of battery voltage,  $V_b$  and the peak supply voltage,  $V_p$ . Based on the partial power ratio, the DC-DC converter process only a portion of total charging power. However, the charger is still able to supply the full charging power to the battery, using the new TPC at front-end.

The proposed TPC operates in two distinct modes, i.e., mode-1 ( $v_{in} < V_b$ ) and mode-2 ( $v_{in} > V_b$ ), Fig. 3(a)–(d) show the converter operation over one switching cycle. The detail description of these two switching states, during each mode, is given as follows.

**Mode-1 ( $v_{in} < V_b$ ):** During this mode, switch  $S_w$  keep in ON state, which makes the diode  $D_1$  in reverse bias. As shown in Fig. 3(a), for the first switching state, the inductor,  $L_i$  starts storing the energy through  $S_w$  and  $S_{wL}$ , as both the switches are conducting. The lower capacitor,  $C_L$  supplies the battery charging current directly using single stage conversion. The diodes  $D_1$  and  $D_2$  both are in OFF state.

Similarly, during the second switching state, switch  $S_{wL}$  is turned OFF, while switch  $S_w$  is still conducting. This makes the diode  $D_2$  forward biased. As shown in Fig. 3(b), the inductor,  $L_i$  starts releasing the stored energy through the diode  $D_2$  and the capacitor,  $C_L$ . Most of the charging power is supplied through the lower port capacitor  $C_L$  during this instant too. Therefore, during mode-1, complete charging power is given by the TPC directly.

**Mode-2 ( $v_{in} > V_b$ ):** As shown in Fig. 2(b), during mode-2, switch  $S_{wL}$  is completely OFF during both the switching states, while, switch  $S_w$  is switching ON and OFF, repeatedly.

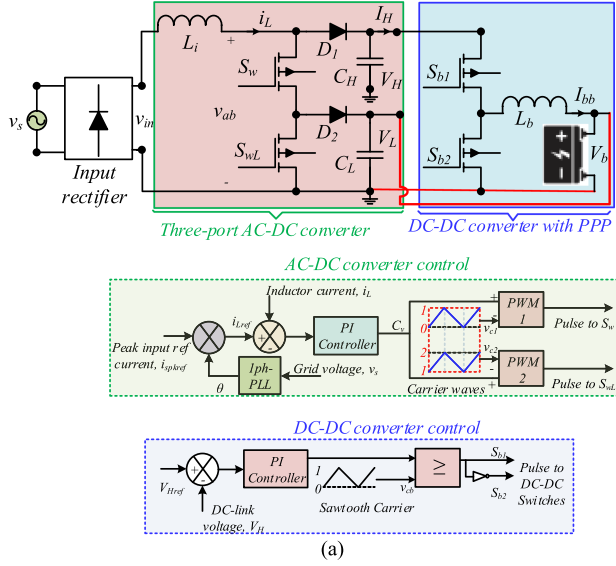


Fig. 2. Proposed PPP converter based fast charger (a) configuration and control. (b) Pulse generation and switching waveforms.

For the first switching state, as shown in Fig. 3(c), \$S\_w\$ is ON and \$S\_{wL}\$ is turned OFF. Therefore, diode \$D\_1\$ remains in OFF state and diode \$D\_2\$ is turned ON. The inductor \$L\_i\$ starts storing the energy through the switch \$S\_w\$ and diode \$D\_2\$ with a voltage difference of \$v\_{in}\$ and \$V\_b\$. The charging power to the battery is provided through the lower capacitor \$C\_L\$. During the second switching state, switch \$S\_w\$ is turned OFF, while the switch \$S\_{wL}\$ is already turned OFF. As shown in Fig. 3(d), the diode \$D\_1\$ now comes in conducting state. The inductor together with the input voltage supplies the required charging power to the battery via DC-DC converter and using the two-stage power conversion.

Therefore, during mode-2, the charging power is shared by the upper and lower port capacitors. However, this sharing is not equal for the capacitors, \$C\_H\$ and \$C\_L\$, but depends on the voltages \$V\_H\$ and \$V\_L\$. Therefore, even if \$v\_{in} > V\_b\$, during mode-2 also, most of the power is transferred to the battery directly through TPC.

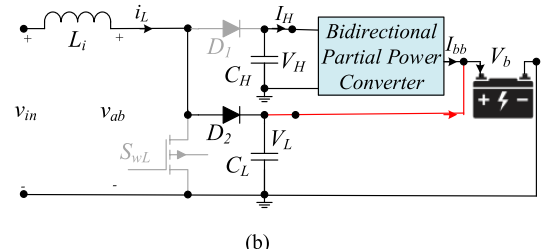
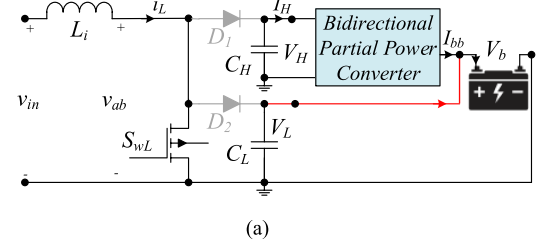


Fig. 3. Converter/Charger operation over one switching cycle during (a)-(b) Mode-1. (c)-(d) Mode-2.

During two modes, applying the volt-second balance for the boost inductor \$L\$, the correlation among input voltage \$v\_{in}\$, \$V\_b\$ and \$V\_H\$ during mode-1 and 2, is given as follows.

$$v_{in} = \begin{cases} \text{Mode 1} & V_b(1 - d_2) \\ \text{Mode 2} & V_b d_1 + (V_b + V_H)(1 - d_1) \end{cases} \quad (1)$$

where \$d\_1\$ and \$d\_2\$ represent the duty ratios for TPC switches \$S\_w\$ and \$S\_{wL}\$, respectively. Further, the expressions for \$d\_1\$ and \$d\_2\$ are obtained as,

$$d_1 = \begin{cases} \text{Mode 1} & 1 \\ \text{Mode 2} & 1 - \frac{v_{in} - V_b}{V_H} \end{cases} \quad (2)$$

$$d_2 = \begin{cases} \text{Mode 1} & 1 - \frac{v_{in}}{V_b} \\ \text{Mode 2} & 0 \end{cases} \quad (3)$$

Therefore, it is obvious that when \$S\_w\$ is continuously ON, \$S\_{wL}\$ is switching on and off (mode-1 operation). However, when \$S\_w\$

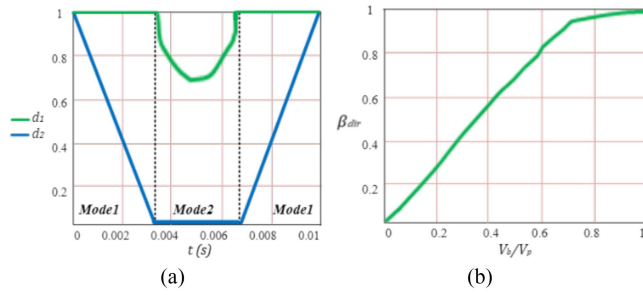


Fig. 4. Graphical change in, (a) duty cycles,  $d_1$  and  $d_2$ , and (b) direct power transfer ratio.

is switching,  $S_{wL}$  remains completely off (mode-2 operation) during a switching cycle. Considering the above expressions and the voltages  $v_s = 220$  V,  $V_b = 270$  V, and  $V_H = 130$  V, the graphical change in the duty ratios  $d_1$  and  $d_2$  is shown in Fig. 4(a). Thus, there is only one high frequency switch is operating over a switching cycle.

Considering  $T_s$  as the switching period for TPC and following the switching sequence during Mode-1 and Mode-2, the expression for the current ripple in  $L$  is given as,

$$\Delta I = \begin{cases} \text{Mode 1} & \frac{v_{in}}{L} d_2 T_s \\ \text{Mode 2} & \frac{v_{in} - V_b}{L} d_1 T_s \end{cases} \quad (4)$$

Substituting the value of  $v_{in}$  from (2) into (4), the current ripple is obtained as,

$$\Delta I = \begin{cases} \text{Mode 1.} & \frac{V_b}{L} (1 - d_2) d_2 T_s \\ \text{Mode 2.} & \frac{V_H}{L} (1 - d_1) d_1 T_s \end{cases} \quad (5)$$

Using (5), for a given value of  $V_b$  and  $V_H$ , the maximum value of  $\Delta I$  is achieved at  $d_1 = 0.5$  or  $d_2 = 0.5$ . Therefore, as per the duty cycle variations in Fig. 4(a), since the dip in  $d_1$  is seen to be 0.7, the peak value of ripple  $\Delta I$  is achieved at  $d_2 = 0.5$ .

Considering the proposed TPC as lossless and harmonic free, the expression for the instantaneous supply power is given as,

$$p_{in}(t) = v_{in} i_{in} = \frac{V_p I_p}{2} (1 - \cos 2\omega t) \quad (6)$$

Where,  $V_p$  and  $I_p$  represent the maximum value of the AC supply voltage and current, respectively. Referring to Fig. 3(d), the mains power is coupled to  $C_H$  only during Mode-2 and when the diode  $D_1$  is conducting. Therefore, the capacitor  $C_H$  power, which is transferred to the bidirectional converter at next stage, is represented as,

$$P_H = \int_{\arcsin(V_b/V_p)}^{\pi - \arcsin(V_b/V_p)} (I_p \sin \omega t (1 - d_1) V_H) d\omega t \quad (7)$$

Based on (7), the power processed by the capacitor  $C_L$ , which is directly supplied by the TPC to the battery is obtained as,

$$P_L = \int_0^\pi (p_{in} d\omega t - P_H) \quad (8)$$

The curve for the directly transferred power to the battery is shown in Fig. 4(b) and largely depends upon the ratio of  $V_b$  and  $V_p$ . Therefore, the ratio of direct power to the total converter power is represented by ratio,  $\beta_{dir}$ , which is expressed as,

$$\beta_{dir} = \frac{P_L}{\int_0^\pi p_{in} d\omega t} = \frac{2}{\pi} \left[ \arcsin \frac{V_b}{V_p} + \frac{V_b}{V_p} \cos \left( \arcsin \frac{V_b}{V_p} \right) \right] \quad (9)$$

It is worth to mention that  $\beta_{dir}$  is independent of the DC-link voltage  $V_H$ , therefore, the only constraint for  $V_H$  is that it should be higher than  $V_p$  to provide the unity power factor (UPF) operation over a supply cycle. It should be noted that the capacitor  $C_H$  is designed to tackle the high frequency voltage ripples generated by the converter switching unlike the capacitor  $C_L$ . Therefore, only  $C_L$  uses an electrolytic capacitor, while the capacitor  $C_H$  may use a film capacitor with low capacitance. The design of proposed charger consists mainly the design of two inductors,  $L_i$  and  $L_b$ , and the capacitors  $C_H$ ,  $C_L$ , considering the mode-1 (duty cycle  $d_2$ ) and mode-2 (duty cycle  $d_1$ ) operations. The design expressions and selected values of different components for 6.6 kW rating are summarized in Table II. The symbols and notations are described in the Table II footnote.

Further, the DC-DC converter is bidirectional buck-boost converter, which is simple as well as efficient. The operating principle of this bidirectional DC-DC converter is same as given in literature [23], [24]. With PPP connection, the bidirectional converter operates only to process a fraction of the power. Therefore, the rating and size of the converter is considerably reduced.

### III. CASE STUDY COMPARISON OVER OTHER CHARGERS

To show the distinct feature of proposed charger, a case study comparison of two-port FPP converter-based chargers in literature [3], [4], [11] and proposed three-port PPP converter-based charger is given in Table III. The comparison shows the superiority of proposed charger in terms of higherefficiency, lower switch rating and improved charging speed Note that for 6.6 kW design, despite providing the full charging power to the battery, DC-DC converter in the proposed charger processes only 10% of total power. Remaining power is fed to the battery directly through the front-end TPC and DC-DC converter gets to process only a fraction of battery charging current. Most of the charging current is processed by the TPC using the bypass connection (red line). As a result, the inductor and switch current,  $I_{bb}$  at DC-DC stage is also very low. However, for the other topologies in [3], [4] and [11], DC-DC converter processes full power of 6.6 kW, 1 kW and 1.3 kW, respectively. Therefore, the switch and inductors need to handle full battery current at output. For the proposed charger, the switch current at TPC stage is high, but lower than the topologies in [3], [4] and [11] for 6.6 kW design.

Also, the chargers in literature [3], [4], [11] use soft switching to provide high efficiency in the range of 93-96%. However, proposed TPC based charger with PPP concept achieves 99.2% efficiency even with hard switching. The switch voltage stresses for proposed charger with PPP concept is recorded as 110 V, 290 V for TPC switches  $Sw$ ,  $SwL$  and 400 V for DC-DC

TABLE II  
DESIGN SPECIFICATION AND RATING OF DIFFERENT CIRCUIT COMPONENTS

Parameter	Specifications	Design Expressions
Input Voltage ( $v_s$ )	220V, Single-phase AC	—
Power ( $P_o$ )	6.6kW	—
DC-Link Voltage ( $V_H$ )	400V	—
Battery specifications ( $V_L$ ) / ( $V_b$ )	270V, 50Ah (Li-ion)	—
Switching frequency ( $f_s$ )	20kHz	—
Duty Cycles $d_1$ and $d_2$ [mode-1 (i.e. $V_{in} < V_b$ )]	—	$d_1 = 1, d_2 = 1 - \frac{V_{in}}{V_b}$
Duty Cycles $d_1$ and $d_2$ [mode-2 (i.e. $V_{in} > V_b$ )]	—	$d_1 = 1 - \frac{V_{in}-V_b}{V_H}, d_2 = 0$
inductors ( $L_i, L_b$ ) [mode-1 (i.e. $V_{in} < V_b$ )]	600μH, 1000μH	$\delta I_L = \frac{V_{in}d_2T_s}{L_i}; \delta I_{Lb} = \frac{V_Hd_2T_s}{L_b}$
inductors ( $L_i, L_b$ ) [mode-2 (i.e. $V_{in} > V_b$ )]	—	$\delta I_L = \frac{V_{in}-V_b d_1 T_s}{L_i}; \delta I_{Lb} = \frac{V_H-V_b d_1 T_s}{L_b}$
Capacitors ( $C_H, C_L$ )	47μF, 2200μF	$C^L = \frac{P_{in}}{4V_b \delta V_b}$

<sup>a</sup>  $d_1$ = duty cycle of switch  $S_w$ ,  $d_2$  = duty cycle of switch  $S_{wL}$ ,  $\delta I_L$  = current ripple in inductor  $L$ ,  $\delta I_{Lb}$  = current ripple in inductor  $L_b$ ,  $T_s$  = switching period,  $P_{in}$  = input power,  $C_H$  = Upper port capacitance,  $C_L$  = lower port capacitance,  $\delta V_b$  = voltage ripple in capacitor  $C_L$ .

TABLE III  
CASE STUDY COMPARISON WITH OTHER TWO-PORT CONVERTER BASED CHARGERS IN LITERATURE

Topology/ Attributes	Charger Topology			
	Converter-1 [3]	Converter-2 [4]	Converter-3 [11]	Proposed
DC bus voltage	400V	300V	250-400V	400V
Battery nominal voltage	330V	320V	250V	270V
Charging current	10A	2.38A	2.8A	23A
Switch voltage stresses in AC-DC and DC-DC stage	500V,600V,400V	300V,600V,600V	300V,100V,650V	110V,290V,400V
Switch current stress (AC-DC)	50A	10A	5-10A	40A
Type of switch	Si	Si	SiC	Si
Total power	6.6kW	1kW	1.3kW	6.6kW
Test input voltage	220V,50Hz	110V,60Hz	85-265V,50/60Hz	220V,50Hz
AC-DC converter power	6.6kW	1kW	1.3kW	6.05kW
DC-DC converter power	6.6kW	1kW	1.3kW	550W
Efficiency	93.6%	95.4%	95.8%	99.2%
Size/power density (W/in <sup>3</sup> )	13.1	18.51	4.012	11.9
Cost (USD)	605.7	485.5	1122	285.93
Charging time (for 50Ah battery)	6-7hrs	more than 10 hrs	more than 10 hrs	2-2.5hrs
Soft switching	Yes	Yes	Yes	No
Control Complexity	Yes	Yes	Yes	No

converter switches, Sb1, Sb2, which is much lower than the chargers in [3], [4], [11]. Further the chargers shown in [3] is designed for 10 A battery current, while the charger in [4], [11] provides 2.3 A/2.8 A, which takes longer to charge a 50 Ah battery. The proposed charger provides 23 A current to the battery which reduces the battery charge time as compared to the other solution in the literature. The total component count is also

fewer in case of proposed charger than those in [3], [4], [11]. It is worth to mention that the main challenge in implementing the proposed PPP based charger is seen with the selection of battery voltage  $V_b$  and DC-link voltage  $V_H$ . As mentioned in operating principle, for appropriate operation during mode-1 and 2,  $V_b$  should be less than  $V_{in \max}$ , i.e., the peak battery voltage is always less than 311V for 220 V AC supply. Further, since the

AC-DC topology is boost type,  $V_H$  should be more than  $V_{in\ max}$ , i.e., cannot not be less than 400 V.

#### IV. CONTROL STRATEGY

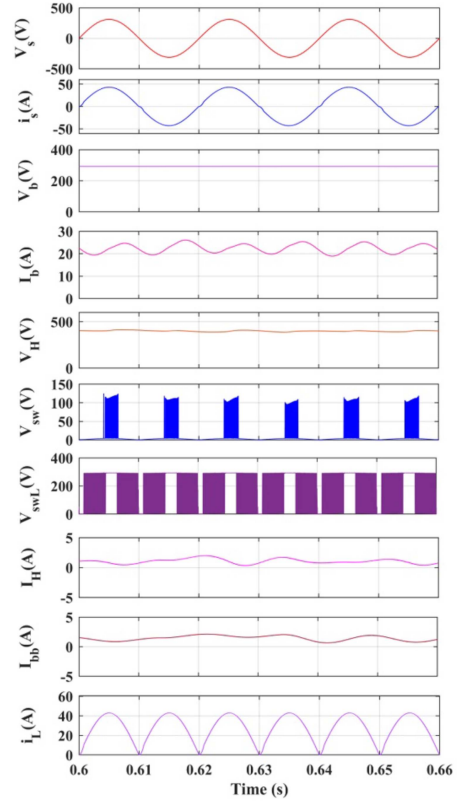
The control strategy for the proposed charger aims at maintaining the UPF operation of the charger, as well as, ensuring the maximum power is transferred directly using single-stage conversion. As shown in Fig. 2(a) and (b), to maximize the direct power through the TPC and to minimize the power processed by DC-DC stage, a dual carrier based PWM strategy is used in this work. As shown in Fig. 2(b), the control output from current PI controller,  $C_v$  is compared with two carriers,  $v_{c1}$  and  $v_{c2}$ . The amplitude of carrier  $v_{c2}$  is biased by the peak amplitude of  $v_{c1}$ . Using this modulation strategy, the proposed TPC has two distinct operating modes based on the relationship between the battery voltage,  $V_b$  and the rectified AC voltage,  $v_{in}$ . When  $v_{in} < V_b$ , the control output,  $C_v$  is greater than the carrier,  $v_{c1}$  and the TPC operates in mode-1. The control output  $C_v$  is modulated by the upper carrier,  $v_{c2}$  only, and hence, switch  $S_w$  is always ON during mode-1. Therefore, the diode  $D_1$  keeps in OFF state, throughout this mode. However, switch  $S_{wL}$  keeps switching ON and OFF during this mode. Similarly, when  $v_{in} > V_b$ , the control output  $C_v$  is lower than the carrier,  $v_{c2}$  and the TPC operates in mode-2. Therefore, the control output  $C_v$  intersects the lower carrier,  $v_{c1}$ , which means that the switch  $S_{wL}$  remains in OFF state. However, the switch  $S_w$  keeps switching ON and OFF, ensuring most of the charging power is processed through the lower port or TPC directly.

#### V. RESULTS AND DISCUSSION

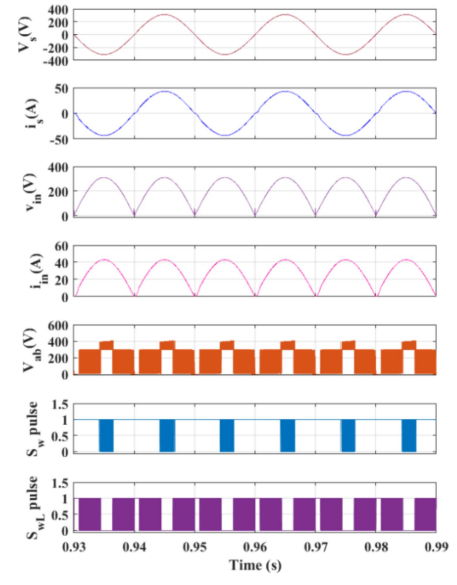
The performance of proposed charger with PPP is assessed and validated using MATLAB/Simulink. The simulation results under steady state condition as well as dynamics in supply voltage and the battery current are discussed as below.

##### A. Simulated Performance

The performance of proposed charger is validated at rated supply voltage of 220 V, 50 Hz. Fig. 5 shows the steady state performance of the three-port converter with the waveform of supply voltage  $v_s$ , supply current  $i_s$ , battery voltage  $V_b$  and the charging current  $I_b$ . Following the specifications in Table II, the battery nominal voltage  $V_b$  (or  $V_L$ ) is selected as 270 V and the charging current  $I_b$ , at rated power of 6.6 kW is 23 A. The DC bus voltage is controlled at 400 V, which is following the requirements of  $V_H > v_{in} > V_b$ , and required for an in-phase supply current regulation. The peak voltage across the TPC devices  $S_w$  and  $S_{wL}$  are recorded as, 110 V ( $V_H - V_b$ ) and 290 V (for  $V_b$  at 60% SOC), respectively, which is quite low as compared to the conventional two stage charger with full power processing. It is worth to note from the waveforms of supply current,  $I_H$  and output current,  $I_{bb}$  that the DC-DC stage processes only 550 W (2.3 A i.e., 10% of total battery current), whereas, the charger is still charging the battery with rated  $I_b = 23$  A at the output. Therefore, it is obvious that almost 90% power is transferred



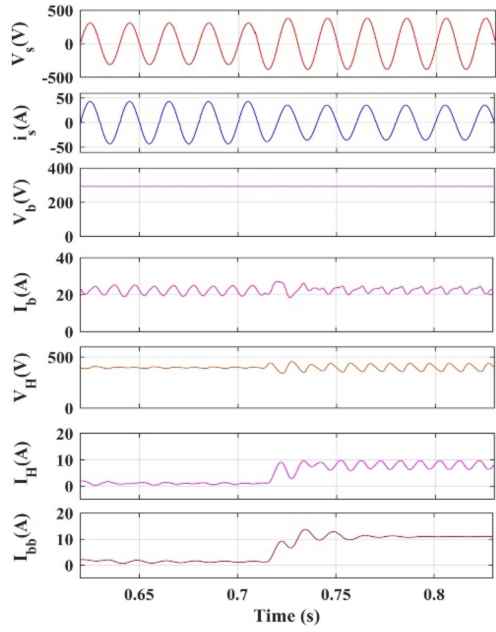
(a)



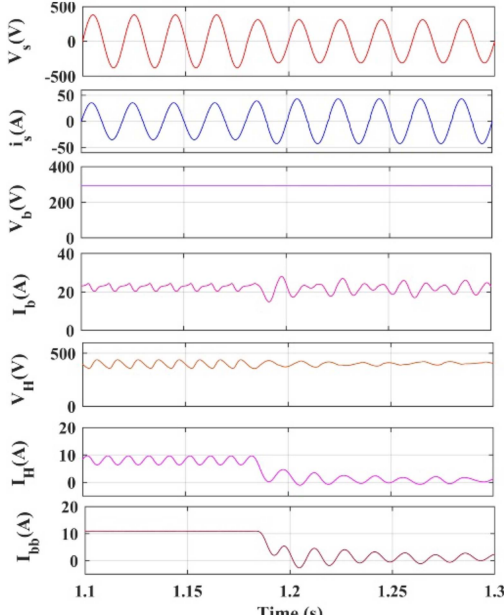
(b)

Fig. 5. Simulated Performance of proposed fast charger during steady state condition, showing waveforms of (a) input and output side quantities with switch voltage, and (b)  $v_{in}$ ,  $i_{in}$  and pole voltage,  $V_{ab}$  with respect to gate pulses to  $S_w$  and  $S_{wL}$ .

to the battery directly using front-end TPC. This directly transferred power largely depends upon the ratio of battery voltage,  $V_b$  and, the peak supply voltage,  $V_p$ . Further, the ripple in battery current,  $I_b$  is seen to be 2.5 A peak, well within the limit for 50 Ah battery and follows the battery ripple current standard NEMA



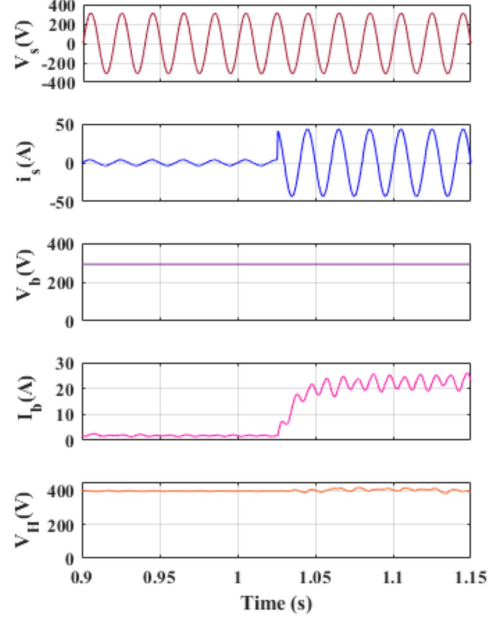
(a)



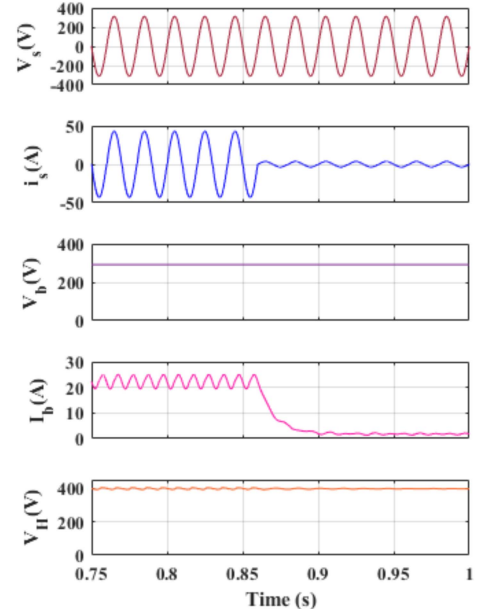
(b)

Fig. 6. Simulated Performance of proposed fast charger during change in  $v_s$  (a) from 220 V–270 V, and (b) from 270 V–220 V.

(National Electrical Manufacturers Association) PE5 [25], [26]. Further, as shown in Fig. 5(b), the waveforms of rectified voltage  $v_{in}$ , rectified current  $i_{in}$  for proposed TPC corresponding to the switch  $S_w$  and  $S_{wL}$  pulses are obtained as per the analysis. It is verified from the pulse waveforms that during mode-1,  $S_w$  remains on all the time, while  $S_{wL}$  is switching ON and OFF. During mode-2,  $S_w$  is switching ON and OFF, while  $S_{wL}$  remains 0 for complete duration. The pole voltage,  $v_{ab}$  is seen to be varying from 400 V–270 V–0 V and hence, giving a three-level voltage, as discussed in operating principle.



(a)



(b)

Fig. 7. Simulated performance of proposed fast charger during (a) startup condition, and (b) shut-down condition.

For comparison, a 6.6 kW conventional 2-port converter based charger with DC-link voltage of 300 V–400 V, and with the charging current as low as 2.3 A–10 A, is considered [3], [4], [11]. For these chargers, the device voltage stress at AC-DC as well as DC-DC stage lies in the range of 400 V–650 V, which restricts the use of these chargers for fast charging. However, using these same switches with the proposed charger enables more charging current for the battery at DC-DC converter end. Further, these chargers in literature achieve 96% efficiency with soft switching, however, proposed charger achieves even higher

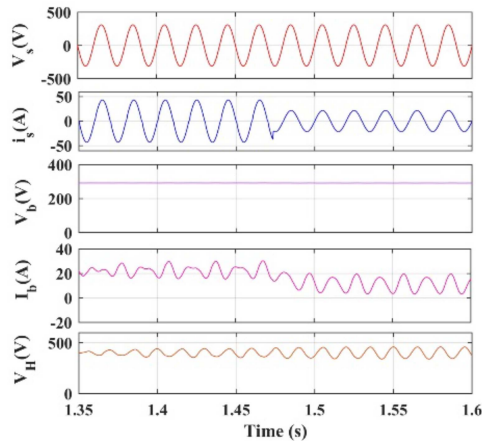


Fig. 8. Simulated performance of proposed fast charger during change in load i.e.,  $I_b$  changes from full load to half load.

efficiency with hard switching due to direct power transfer to the battery from TPC. The rated full-load efficiency of the charger is seen to be as high as 99.2% without any soft-switching used in the circuit.

The performance of proposed TPC and PPP converter-based charger is assessed under the transients in supply voltage. As mentioned earlier, variation in supply voltage changes the percentage of directly transferred power through the TPC, as the portion of current flowing through DC-DC converter changes. This is because the directly transferred power largely depends upon the ratio of battery voltage,  $V_b$  and, the peak supply voltage,  $V_p$ . This is validated through Fig. 6(a), when supply voltage is increased from 220 V–270 V. The battery current as well as  $V_H$  remain tightly regulated, however, the supply current,  $i_s$  reduces to maintain the power flow through the circuit. Therefore, the current taken by the TPC reduces or the portion of direct power transfer is less. This clearly increase the current entering to the DC-DC converter to 50% of total battery current as the direct power transfer to the battery reduces with increase in the peak line voltage. Fig. 6(b) further shows the vice versa case for the change in line voltage from 270 V–220 V. The input current increases with the corresponding decrease in the power processed by the DC-DC converter.

The robust performance of proposed charger during circuit start-up and shut-down is analyzed by applying the change in charging power from zero to rated and vice-versa. As shown in Fig. 7(a), as soon as the charging power rises from zero to rated value (23 A), the battery current rises accordingly without any inrush in supply current. The supply current also increases along with the battery current to show the smooth transition during start-up process. Similarly, as per Fig. 7(b), during shut-down performance, as soon as the battery current observes a dip from rated 23 A to 0, the supply current reduces to very low value to sustain a smooth transition without any inrush. Fig. 8 demonstrates the charger performance under change in battery current from full load to half load for rated supply voltage. It is worth to note that as the battery current changes from 23 A to 11.5 A, the line current is seen to be reduced from the rated

TABLE IV  
PROTOTYPE PARAMETERS/TEST EQUIPMENT DETAILS

Components/Parameter	Parameter Value	Equipment Model No/Part No.
Input supply voltage	-	Single phase AC supply, 220V
DC electronic load	-	BK precision 8522 2400W programmable electronic load to emulate 300V,5A battery
Oscilloscope (DSO)	-	Tektronix DPO 4054B, digital phosphor oscilloscope
Current probe/voltage probe	-	TCP0030 120 MHz VPI 30A, AC/DC current probes/ TDP0500 500MHz VPI differential voltage probes
Current sensor/voltage sensor	-	USM-3IV, Taraz Technologies
Output Inductor $L_b$	1mH	Magnetics: toroidal core 77726A7, 120 turns, AWG 18
TPC switch converter, $S_w$	--	Fairchild semiconductor FQA44N30, $v_{ds0}=1.5V$ , $r_{ds}=55m\Omega$ , $t_r=470ns$ , $t_f=280ns$
TPC switch converter, $S_{wL}$	--	Infineon, SPW32N50C3, $v_{ds0}=1V$ , $r_{ds}=11m\Omega$ , $t_r=30ns$ , $t_f=10ns$
DC-DC converter switches, $S_{b1}, S_{b2}$	--	Infineon SPW32N50C3, $v_{ds0}=1V$ , $r_{ds}=11m\Omega$ , $t_r=30ns$ , $t_f=10ns$
Diode, $D_{1,2}$	--	Fairchild semiconductor, $V_{Fpn}=1.4V$ , $r_{Dpn}=2m\Omega$
Switching frequency, $f_s$	20kHz	
TPC capacitors ( $C_H, C_L$ )	47µF, 500µF	1 Nichicon, MHBS355470KJS and 4*120µF, Aluminium electro.cap.
Output capacitor, $C_b$	500µF	Aluminium electrolytic capacitor

value. However, the DC bus voltage  $V_H$  still remains tightly regulated, irrespective of the change in load current. Therefore, the proposed charger is able to sustain 50% change in load current without any disturbance in operation.

### B. Experiment Verification

To verify the proof-of-concept, a scaled down lab prototype for 1.5 kW is built and tested under various operating conditions. The design parameters for the prototype are given in Table IV and the prototype picture is shown in Fig. 9. The proposed charger is controlled using digital signal processor (DSP) kit TI TMS320F28379D. The supply voltage,  $v_s = 220 \text{ V}/50 \text{ Hz}$  is given through a variable 1 $\phi$  auto-transformer, and the battery voltage,  $V_b = 270 \text{ V}$  is connected using programmable DC-electronic load. It is worth to mention that the main challenge in implementing the proposed PPP based charger is seen with the selection of battery voltage  $V_b$  and DC-link voltage  $V_H$ . As mentioned in operating principle, for appropriate operation during mode-1 and 2,  $V_b$  should be less than  $V_{in \max}$ , i.e., the peak battery voltage is always less than 311V for 220 V AC supply. Further, since the AC-DC topology is boost type,  $V_H$  should be more than  $V_{in \ max}$ , i.e., cannot not be less than 400 V.

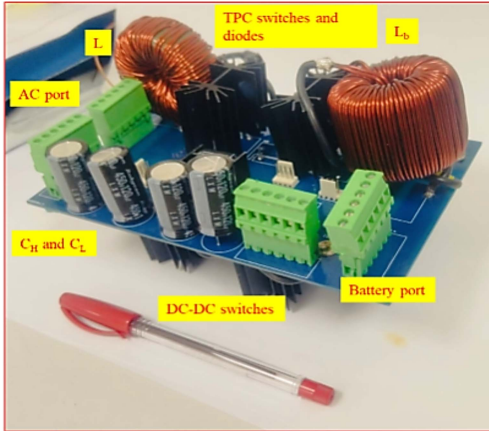


Fig. 9. Picture of the laboratory prototype.

Referring to Fig. 4(b) and the experimental results shown in Fig. 10(a) verify the value of the ratio  $\beta_{dir}$  as 90%, while the battery is charging in CC mode with current of 5.1A. Hence, the rating of DC-DC stage is reduced to 10% of total charging power required by the battery, as shown in Fig. 10(b), i.e., the current supplied by DC-DC stage is 0.51A (10% of 5A). To maintain the UPF operation over a line cycle, the DC-link voltage  $V_H$  is recorded as 400 V, as shown in Fig. 10(c), which is higher than the battery voltage,  $V_b$  (or  $V_L$ ). The DC-DC stage is implemented using the open-loop as it operates with constant voltage gain. The experiment waveforms of  $V_g$  and  $V_{gL}$  for two switches in TPC are recorded as per Fig. 11(a) and the pole voltage,  $v_{ab}$  shows three voltage levels as 0,  $V_b$  and  $V_H$ . The proposed TPC switches between mode-1 and mode-2 during each half line cycle, as shown in Fig. 11(b).

The proposed TPC input current,  $i_{in}$  follows the input voltage  $v_{in}$ , and is exactly in-phase. To verify the proposed charger robustness, the recorded waveforms of change in supply voltage from 220 V–270 V and, vice versa, are given in Fig. 12(a) and (b). For the sudden increase and decrease in the supply voltage, the supply current observes a corresponding decrease and increase respectively, to maintain the charger power balance. However, the DC-link voltage,  $V_H$  is well regulated at 400 V. The battery voltage and current are observed as per the rated value, while the DC-link current or DC-DC converter current changes as the ratio of  $V_b$  and the peak supply voltage,  $V_p$  changes. As  $V_p$  increases,  $i_p$  (TPC current) reduces and the direct power transfer ratio  $\beta_{dir}$  reduces. Therefore, the change in DC-DC converter current is observed from 0.51 A to 2 A, as shown in Fig. 12(a). Similarly, as shown in Fig. 12(b), for decrease in  $V_p$ ,  $\beta_{dir}$  increases implying to the change in DC-DC converter current is observed from 2 A to 0.51 A.

Further, to highlight the contribution of proposed topology over other charging solutions in literature as given in Table I, a comparative analysis showing the higher charging speed, improved efficiency and the reduced cost over the FPP DC-DC converter-based topologies is discussed, which are illustrated in Fig. 13(a)–(d). The improved performance of the proposed

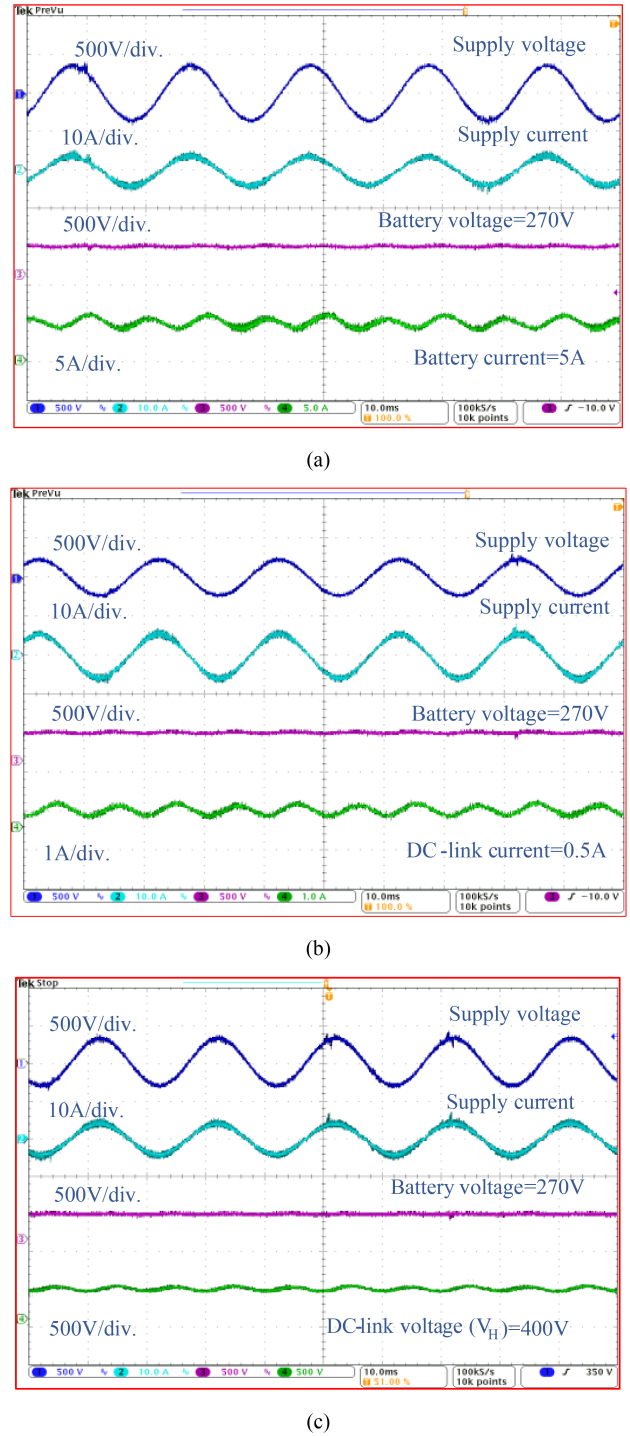


Fig. 10. Experiment waveforms at steady state. (a) Battery charging in CC mode with 5 A current, (b) 10% reduction in DC-DC stage rating, i.e., DC-link current,  $I_H$ , and (c) DC-link voltage,  $V_H$  maintained at 400 V.

charger is characterized by the change in efficiency curve (simulated) over different supply voltages, i.e., at 200 V, 220 V and 240 V AC. As shown in Fig. 13(a), the peak simulated efficiency of the proposed charger at rated 220 V, is observed as 96.7%, which is significantly higher than the chargers with full-power processing and hard-switching.

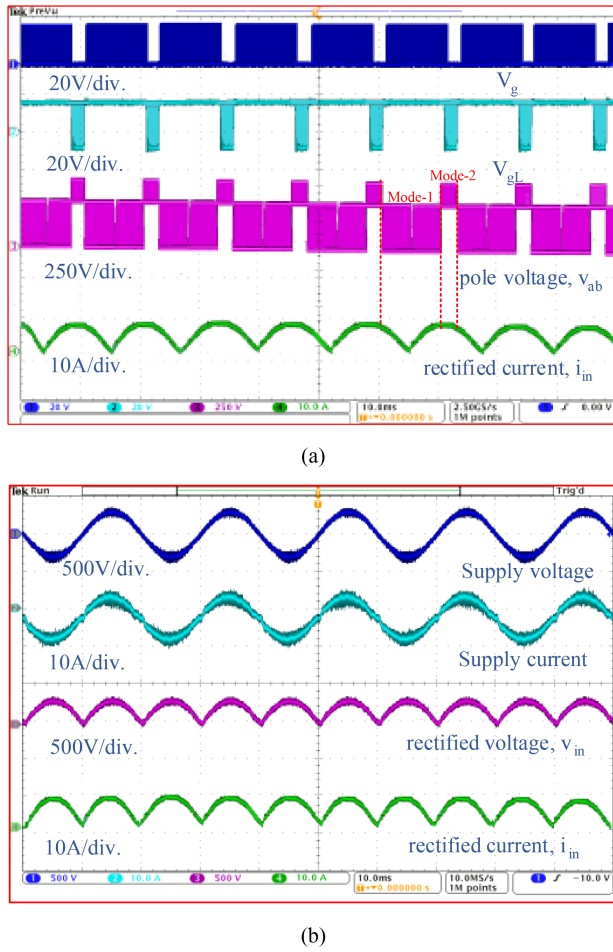


Fig. 11. Experiment waveforms at steady state. (a) Pole voltage,  $v_{ab}$ , and (b) rectified voltage and current showing the mode transitions over half line cycle.

Now, referring to Table I, all the nine topologies can be summarized under three categories: conventional single-stage chargers (with FPP DC-DC converters) [5], conventional two-stage chargers (with FPP DC-DC converters) [3, 4, 6, 7, 8, 9, 10, 11] and proposed charger with PPP DC-DC converters. Keeping this classification into consideration, the change in battery SOC over time for 50 Ah Li battery is compared to estimate the charging speed with all three configurations for given DC-link voltage. As shown in Fig. 13(b), since the single-stage chargers in literature are designed for 50 V output, the slope of rise in SOC over time is slowest, i.e., the charging speed is lowest for these chargers. Further, the two-stage chargers are designed to operate at 300 V DC-link voltage leading into slightly higher charging speed or reduced charge time over the conventional single stage but less than the proposed charger, which is designed to operate at 400 V DC-link voltage. The charge time for proposed charger is limited to 1 hour, which implies the charging speed is increased as compared to conventional solutions.

Moreover, as per Fig. 13(c), the efficiency of proposed charger with TPC and PPP connection at DC-DC stage is seen to be highest on account of reduced size of TPC switches, reduced switching loss due to 3-level output voltage and further, due to reduced rating of DC-DC stage with PPP connection. The

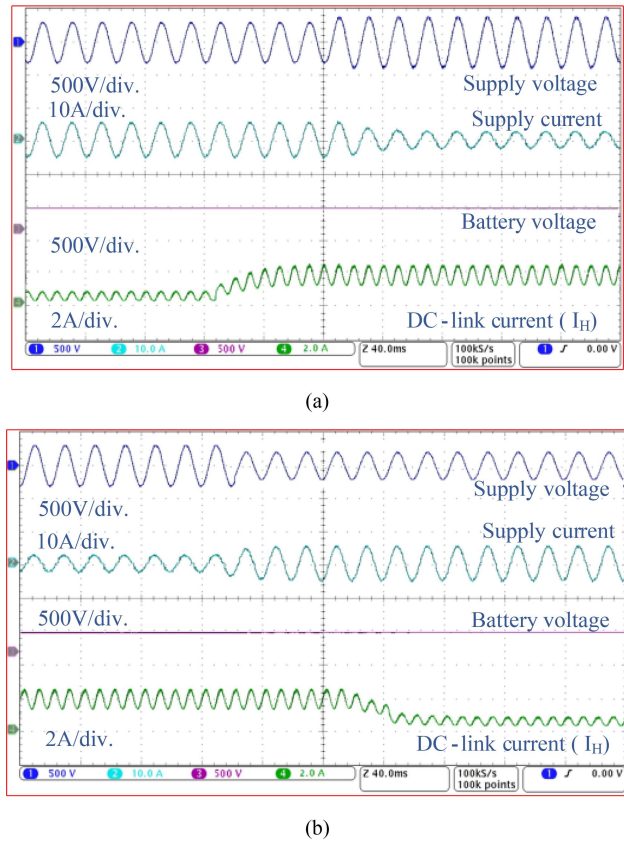


Fig. 12. Experiment waveforms showing the variation in DC-DC stage rating during transients in supply voltage, (a) from 220 V–270 V, and (b) 270 V–220 V.

conventional two-stage topologies in consideration [3], [4], [6], [7] exhibit lowest efficiency ranges due to use of more components and hard-switching. Further, the other contemporary two-stage topologies with soft-switching [8], [10], [11] show slightly higher efficiency than those with hard switching, but still less than the proposed charger with PPP, as the DC-DC stage is rated at full-power processing (FPP).

Further, a detailed cost comparison of proposed charger with PPP is given in Fig. 13(d) over the conventional two-stage topologies with FPP [3], [4], [6], [7] under consideration in Table I. It is obvious from Table I that most of the two-stage contemporary solutions have a greater number of components in the circuit than the proposed solution. Apart from that due to full-power processing at DC-DC stage and two-port structure at AC-DC stage, the rating of components, switches and DC-DC converter is higher, which leads to increased cost as compared to proposed charger with PPP. Most of conventional charging solution use SiC components to achieve high power density design, the most crucial for on-board fast chargers. Significant cost reduction is seen with proposed charger as due to reduced switch voltage stress at AC-DC stage and reduced rating of DC-DC converter, the SiC active components can be replaced with Si active components, which is one of the main reasons for higher cost of conventional charging solution, e.g., topology [11].

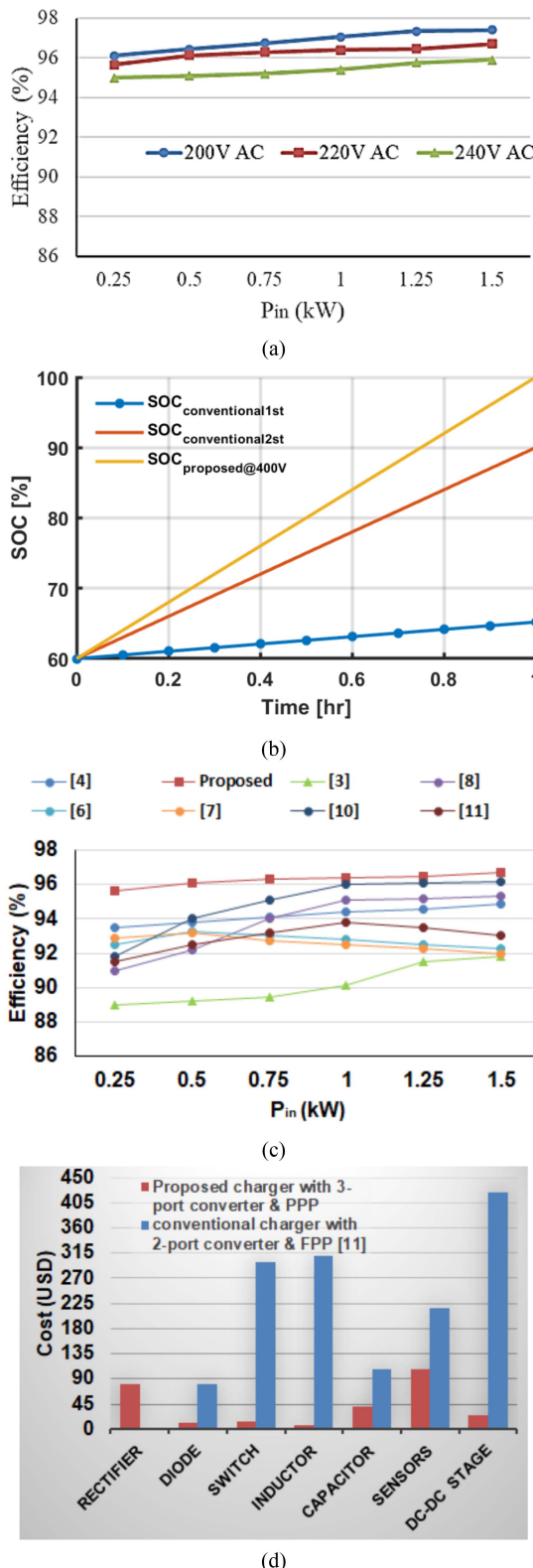


Fig. 13. Comparative analysis of proposed fast charger over the other solutions in literature. (a) Efficiency at different supply voltages (b) charging speed (c) efficiency over state-of-art chargers with full power processing (FPP) (d) cost comparison with [11].

## VI. CONCLUSION

A new fast charger configuration based on three-port converter (TPC) with partial power processing (PPP) is presented in this work. This new three-port converter with PPP has enabled reduced device voltage stress at AC-DC stage, as well as reduced current stress at DC-DC stage. As a result, the size and cost of the charger is significantly reduced, as well as the efficiency is improved. The proposed charger transfers most of the power directly to the battery using front-end TPC, however, only a fraction of the power is processed through the DC-DC stage. Consequently, even without soft-switching, the efficiency of proposed charger is higher than compared to the state-of-art chargers discussed in the paper. The peak efficiency of the proposed charger is recorded as 96.13%, which is quite attractive for hard-switched chargers. It is observed that the rating of DC-DC converter is reduced to 10% of the rating in state-of-art full power processing (FPP) based chargers. Using the same power rating as in conventional two-port converter, proposed charger ensures increased charging speed, comparatively, which is achieved on account of operation of proposed charger at higher DC-link voltage.

## VII. FUTURE WORK

Along with the current requirements for high efficiency and high-power density, a new set of regulation for power efficiency as well as system performance with compact and cost-effective alternatives during bidirectional charging of battery with proposed charger might be planned and enforced in the upcoming era. These regulatory requirements may open wider platform for new research opportunities which helps the researchers and industries to combat the new research problems. Based on these regulatory and research gaps, the future scope for the proposed work is enlisted as follows.

- 1) The efficiency and power level could be increased to provide fast charging to the battery with off-board configuration. Variable frequency control and modular construction approaches might aid in the optimization of the efficiency curve, further.
- 2) The use of soft switching circuits for further reduction in switch stress as well as losses.
- 3) Using interleaved version of proposed three-port AC-DC converter may result in better ripple characteristics.
- 4) Using SiC and GaN devices as active components leads to better converter power density at high power owing to reduced voltage drops and switching transition times.
- 5) As a future work, proposed charger can be used as an integrated converter (with diode replaced by switches) for bidirectional charging, which further can be extended to couple with motor drives like BLDC and SRM motor drive for EV propulsion.
- 6) Further, certain dynamic condition of battery and vehicle can be analysed using proposed charger, leading to wider future innovation to the researchers.

## REFERENCES

- [1] H. Tu, H. Feng, S. Srdic, and S. Lukic, "Extreme fast charging of electric vehicles: A technology overview," *IEEE Trans. Transp. Electric.*, vol. 5, no. 4, pp. 861–878, Dec. 2019.
- [2] M. Safayatullah, M. T. Elrais, S. Ghosh, R. Rezaei, and I. Batarseh, "A comprehensive review of power converter topologies and control methods for electric vehicle fast charging applications," *IEEE Access*, vol. 10, pp. 40753–40793, 2022.
- [3] J. Y. Lee and H.-J. Chae, "6.6-kW onboard charger design using DCM PFC converter with harmonic modulation technique and two-stage DC/DC converter," *IEEE Trans. Ind. Electron.*, vol. 61, no. 3, pp. 1243–1252, Mar. 2014.
- [4] H. Wang, S. Dusmez, and A. Khaligh, "Design and analysis of a full-bridge LLC-based PEV charger optimized for wide battery voltage range," *IEEE Trans. Veh. Technol.*, vol. 63, no. 4, pp. 1603–1613, May 2014.
- [5] S. Dutta, S. Gangavarapu, A. K. Rathore, R. K. Singh, S. K. Mishra, and V. Khadkikar, "Novel single-phase Cuk-derived bridgeless PFC converter for on-board EV charger with reduced number of components," *IEEE Trans. Ind. Appl.*, vol. 58, no. 3, pp. 3999–4010, May/Jun. 2022.
- [6] A. Singh, J. Gupta, and B. Singh, "Design and control of two stage battery charger for low voltage electric vehicles using high gain buck-boost PFC AC-DC converter," *IEEE Trans. Ind. Appl.*, vol. 59, no. 5, pp. 6125–6135, Sep./Oct. 2023.
- [7] A. Singh, J. Gupta, and B. Singh, "Bridgeless modified high-step-up gain SEPIC PFC converter based charger for light EVs battery," *IEEE Trans. Ind. Appl.*, vol. 59, no. 5, pp. 6155–6166, Sep./Oct. 2023.
- [8] A. Dixit, S. Gangavarapu, and A. K. Rathore, "High-efficiency discontinuous current-mode power factor correction-based plug-in battery charger for local e-transportation," *IEEE Trans. Transp. Electric.*, vol. 7, no. 3, pp. 1134–1145, Sep. 2021.
- [9] A. V. J. S. Praneeth and S. S. Williamson, "Modeling, design, analysis, and control of a nonisolated universal on-board battery charger for electric transportation," *IEEE Trans. Transp. Electric.*, vol. 5, no. 4, pp. 912–924, Dec. 2019.
- [10] A. V. J. S. Praneeth, D. Vincent, and S. S. Williamson, "An universal on-board battery charger with wide output voltage range for electric transportation," in *Proc. IEEE Energy Convers. Congr. Expo.*, 2019, pp. 1159–1165.
- [11] H. Karneddi and D. Ronanki, "Analysis and design of a wide output voltage range battery charger for E-mobility applications," *IEEE J. Emerg. Sel. Top. Ind. Electron.*, vol. 5, no. 2, pp. 543–552, Apr. 2024.
- [12] U. Sharma and B. Singh, "A bidirectional onboard charger with multistep constant current charging capability," *IEEE Trans. Transp. Electric.*, vol. 9, no. 1, pp. 1227–1237, Mar. 2023.
- [13] U. Sharma and B. Singh, "Functional link neural network for wide load operation of bidirectional onboard charging system of E-rickshaw," *IEEE Trans. Ind. Appl.*, vol. 58, no. 6, pp. 7668–7679, Nov./Dec. 2022.
- [14] U. Sharma and B. Singh, "A bidirectional bridgeless converter-based electric vehicle charger," *IEEE Trans. Ind. Appl.*, vol. 60, no. 1, pp. 900–909, Jan./Feb. 2024.
- [15] O. Abdel-Rahim, A. Chub, A. Blinov, and D. Vinnikov, "Current-fed dual inductor push-pull partial power converter," in *Proc. IEEE 20th Int. Power Electron. Motion Control Conf.*, 2022, pp. 327–332.
- [16] O. Abdel-Rahim, A. Chub, A. Blinov, and D. Vinnikov, "Series buck-boost partial power converter based on the push-pull converter," in *Proc. 48th Annu. Conf. IEEE Ind. Electron. Soc.*, 2022, pp. 1–5.
- [17] SAE Electric Vehicle and Plug in Hybrid Electric Vehicle Conductive Charge Coupler, Revised, Standard J1772 \_201710, SAE International Warrendale, PA, USA, 2017.
- [18] N. Hassanpour, A. Chub, A. Blinov, and D. Vinnikov, "Comparison of full power and partial power buck-boost DC-DC converters for residential battery energy storage applications," in *Proc. IEEE 16th Int. Conf. Compat. Power Electron., Power Eng.*, 2022, pp. 1–6.
- [19] J. R. R. Zientarski, M. L. d. S. Martins, J. R. Pinheiro, and H. L. Hey, "Series-connected partial-power converters applied to PV systems: A design approach based on step-up/down voltage regulation range," *IEEE Trans. Power Electron.*, vol. 33, no. 9, pp. 7622–7633, Sep. 2018.
- [20] J. Anzola et al., "Review of architectures based on partial power processing for DC-DC applications," *IEEE Access*, vol. 8, pp. 103405–103418, 2020.
- [21] J. Rojas, H. Renaudineau, S. Kouro, and S. Rivera, "Partial power DC-DC converter for electric vehicle fast charging stations," in *Proc. 43rd Annu. Conf. IEEE Ind. Electron. Soc.*, 2017, pp. 5274–5279.
- [22] R. Kushwaha, V. Khadkikar, S. Singh, H. H. Zeineldin, R. Mizouni, and H. Otrok, "An efficient three-port partial power converter based EV on-board fast charger," in *Proc. IEEE Int. Conf. Power Electron., Drives Energy Syst.*, 2022, pp. 1–6.
- [23] F. Caricchi, F. Crescimbini, F. G. Capponi, and L. Solero, "Study of bidirectional buck-boost converter topologies for application in electrical vehicle motor drives," in *Proc. 13th Annu. Appl. Power Electron. Conf. Expo.*, 1998, pp. 287–293.
- [24] M. A. Khan, A. Ahmed, I. Husain, Y. Sozer, and M. Badawy, "Performance analysis of bidirectional DC-DC converters for electric vehicles," *IEEE Trans. Ind. Appl.*, vol. 51, no. 4, pp. 3442–3452, Jul./Aug. 2015.
- [25] (n.d.) [Online]. Available: <http://www.atseries.net/PDFs/JD5013-00.pdf>
- [26] A. D. Kupchinov, Y. P. Gusev, and Y. V. Monakov, "Batteries current ripples in float charge mode," in *Proc. IEEE Conf. Russian Young Researchers Elect. Electron. Eng.*, 2017, pp. 913–915.



**Radha Kushwaha** (Senior Member, IEEE) received the B.Tech. degree in electrical engineering from Gautam Buddha Technical University, Uttar Pradesh, India, in 2012, the M.Tech. degree in electrical engineering from the National Institute of Technology, Durgapur, India, in 2014, and the Ph.D. degree in power electronics with the Department of Electrical Engineering, Indian Institute of Technology (IIT) Delhi, New Delhi, India, in August 2020. She was Visiting Researcher with Advanced Power and Energy Center, Khalifa University, Abu Dhabi, UAE. She was associated with Caterpillar Inc., Bengaluru, India, as a Senior R&D Engineer from May 2021 to Oct 2021. Since October 2021, she has been a Post Doctoral Research Fellow with Khalifa University. Her research interests include power electronics, battery charger systems, power factor correction, and AC-DC and DC-DC power converters.



**Vinod Khadkikar** (Fellow, IEEE) received the M.Tech. degree in power electronics, electrical machines, and drives from the Indian Institute of Technology, New Delhi, India, in 2002, and the Ph.D. degree in electrical engineering from the Ecole de Technologie Supérieure, Montreal, QC, Canada, in 2008. From 2008 to 2010, he was a Postdoctoral Fellow with the University of Western Ontario, London, ON, Canada. In 2010, he was a Visiting Professor with the Massachusetts Institute of Technology, Cambridge, MA, USA. He is currently a Professor with the Department of Electrical Engineering and Computer Science, Khalifa University, Abu Dhabi, UAE. His research interests include applications of power electronics in distribution systems and renewable energy resources, grid interconnection issues, power quality enhancement, active power filters, and electric vehicles. Dr. Khadkikar is a distinguished Lecturer of IEEE Industry Applications Society. He is currently the Co-EiC of IEEE TRANSACTIONS ON INDUSTRIAL ELECTRONICS and an Associate Editor for IEEE TRANSACTIONS ON INDUSTRY APPLICATIONS and IET Power Electronics.



**Shakti Singh** (Member, IEEE) received the B.Sc., M.Sc., and Ph.D. degrees in electrical and computer engineering from Purdue University, West Lafayette, IN, USA, in 2000, 2003, and 2010, respectively. He joined as a Faculty with the Electrical Engineering and Computer Science Department, Khalifa University of Science and Technology, Abu Dhabi, UAE, in 2010. His research interests include semiconductor devices and technologies, artificial intelligence (AI), crowd sensing and sourcing, blockchain, and IoT sensors and networks.



**Hatem H. Zeineldin** (Senior Member, IEEE) received the B.Sc. and M.Sc. degrees in electrical engineering from Cairo University, Giza, Egypt, in 1999 and 2002, respectively, and the Ph.D. degree in electrical and computer engineering from the University of Waterloo, Waterloo, ON, Canada, in 2006. He was with Smith and Andersen Electrical Engineering, Inc., North York, ON, USA, where he was involved in projects involving distribution system designs, protection, and distributed generation. He was a Visiting Professor with the Massachusetts Institute of Technology, Cambridge, MA, USA. He is currently with Khalifa University, Abu Dhabi, UAE, and on leave from the Faculty of Engineering, Cairo University, Cairo, Egypt. His research interests include distribution system protection, distributed generation, and micro grids. Dr. Zeineldin is currently the Editor of IEEE TRANSACTIONS ON ENERGY CONVERSION.



**Hadi Otrok** (Senior Member, IEEE) received the Ph.D. degree in electrical and computer engineering from Concordia University, Montreal, QC, Canada, in 2008. He is currently an Associate Professor position with the Department of Electrical Engineering and Computer Science, Khalifa University, Abu Dhabi, UAE. He is an Affiliate Associate Professor with the Concordia Institute for Information Systems Engineering, Concordia University, Montreal, and an Affiliate Associate Professor with the Electrical Department, Ecole de Technologie Supérieure (ETS), Montreal, QC, Canada. His research interests include the domain of blockchain, reinforcement learning, crowd sensing and sourcing, ad hoc networks, and cloud security. Dr. Otrok co-chaired several committees at various IEEE conferences. He is also an Associate Editor for IEEE TRANSACTIONS ON NETWORK AND SERVICE MANAGEMENT (TNSM), *Ad-Hoc Networks* (Elsevier), and IEEE NETWORK. From 2015 to 2019, he was also an Associate Editor for IEEE COMMUNICATIONS LETTERS.



**Rabeb Mizouni** received the M.Sc. and Ph.D. degrees in electrical and computer engineering from Concordia University, Montreal, QC, Canada, in 2002 and 2007, respectively. She is currently an Associate Professor with the Department of Electrical Engineering and Computer Science, Khalifa University, Abu Dhabi, UAE. Her research interests include the deployment of context aware mobile applications, crowd sensing, Artificial Intelligence, IoT, and Blockchain. Dr. Mizouni is currently an Associate Editor for *IEEE Internet of Things Magazine*.